CYBERNETICS AND PHYSICS, VOL. 13, NO. 3, 2024, 248–260

TRAJECTORY TRACKING CONTROLLER DESIGN FOR QUADCOPTER UNDER DISTURBANCES ENVIRONMENT: USING A HYBRID APPROACH

Sanjay Kumar
Department of Electrical Engineering
National Institute of Technology Kurukshetra
India
sanjay_6180079@nitkkr.ac.in

Lillie Dewan
Department of Electrical Engineering
National Institute of Technology Kurukshetra
India
l_dewan@nitkkr.ac.in

Article history:
Received 09.10.2024, Accepted 26.11.2024

Abstract

The development of a robust tracking controller for autonomous aerial vehicles to reach the desired point has become extremely important, especially when flying in the ground region. This paper proposes a hybrid controller (proportional fractional-order integral derivative sliding surface based on sliding mode control with backstepping (PFOIDSMCBS)) to control the quadcopter to flow the predefined trajectory. The proposed controller is designed to control the attitude, altitude, and angular motion with payload in the presence of external disturbances, wind, and ground effects. The performances of the proposed controller have been compared with the existing SMCBS controller. The simulation results show that the system satisfies the stability condition and is efficient in path tracking. As the vehicle approaches the ground, the simulation indicates a consistent linear increase in the total thrust generated by the rotors. In the landing, the proposed controller reduces settling time by 6.12% compared to SMCBS for the system without load. With a load, it reduces settling time by 5.17% compared to SMCBS. PFOIDSMCBS controller exhibits superior performance over SMCBS in terms of minimizing chattering effects and reducing control effort.

Key words

Quadcopter model, Nonlinear system, Hybrid controller.

1 Introduction

Quadcopters, unmanned aerial vehicles, have attracted significant attention due to their numerous applications [Yacef et al., 2014; Araar and Aouf, 2014]. The quadcopter system an under-actuated system possesses six degrees of freedom (DoF) while having only four control inputs, due to this quadcopters require effective flight control, especially during takeoff, inflight, and landing. The takeoff and landing of quadcopters on the ground surface or any surface have been discussed by many authors [Kumar and Dewan, 2024; Danjun et al., 2015]. Most of the work has been focused on ensuring the quadcopter's safe landing on its target. During flight, as the quadcopter enters or exits the ground effect region, it impacts due to this ground effect. In [Fujita and Shimada, 2007] author has derived equations for the ground effect and provided a methodology to calculate how it influences the quadcopter. First, in 1957, Cheeseman's model derivation the thrust ratio inside and outside the ground effect for a single-rotor helicopter, after that other authors gave the modified Cheeseman's model calculation [Davis et al., 2015]. In [Danjun et al., 2015] author, clarify the behavior of the ground effect on the helicopter as well as quadcopter. Various aspects of the ground effect have been addressed experimentally, mathematically, and computationally by the authors [Sharf et al., 2014]. Quadcopters are also sensitive to wind gusts, which affect the control of the quadcopter and make it dangerous to operate in populated areas. However, there is less research quantifying the wind effects. The literature [Chen et al., 2013; Waslander and Wang, 2009] explains that wind effects increase due to the wind flow interaction with the propellers. Wind gusts taken as a disturbance force vector has been given by [Dikmen et al., 2009; Tran et al., 2015], and the addition of a dynamic wind model in a state-space model of the quadcopter has been represented in [Ambati and Padhi, 2014; Nekoo et al., 2021]. The payload acts as a mass variation of the quadcopter resulting in a loss of commandability. As fuel constitutes a considerable portion of the vehicle's total mass, this problem becomes more apparent [Cho et al., 2020].

Safety, operational reliability, predefined path trajectory tracking, and controlling of the quadcopters have been represented by many researchers in our work [Mori et al., 2008; Watanabe et al., 2008]. Most of the time, linear and nonlinear controllers have been designed by authors to control the performance of the quadcopter [Kumar and Dewan, 2020; Sharma and Lather, 2020]. Different nonlinear controllers have been proposed to address the external disturbances [Sadeghzadeh et al., 2014], wind effect [Ambati and Padhi, 2014], atmospheric disturbances [Alexis et al., 2011], and time-invariant disturbances in [Cho et al., 2020],[Gao and Wang, 2013]. Other control techniques, such as hybrid control [Sahrir and Basri, 2023],[Kumar and Dewan, 2022], have been proposed to mitigate the effect of sensor noise, wind as a shock, external disturbances, and mass variation, etc. In addition, by applying the principles of fractional calculus, the efficacy of sliding mode control (SMC) is improved by the combination of the advantages of both theories. In recent years, there has been various research that has expanded the application of fractional order sliding mode control (FOSMC) to tackle disturbances and uncertainties in quadrotor control. In [Ayad et al., 2019], a continuous-time fractional-order proportional-derivative (PD) controller was introduced. A fractional-order sliding mode controller, utilizing backstepping, has been introduced [Vahdanipour and Khodabandeh, 2019] to alleviate wind disturbances and fluctuations in load moment of inertia. Similarly, a new fractional-order proportional-integral (PI) nonlinear system for quadrotor attitude control was proposed by [Oliva-Palomo et al., 2019]. The authors [Hua et al., 2019] developed a controller based on fractional-order sliding mode theory to address the tracking issue of an uncertain quadrotor with time-varying state constraints.

A model of quadcopter [Bouabdallah and Siegwart, 2005] has been used for the development of the control system. In this paper, an effort has been made to enhance this model by adding various disturbances, aiming to achieve a more comprehensive dynamic model to [Xiong and Zheng, 2014]. This paper design a novel controller that combines the advantages of SMCBS with fractional theory to develop a fractional order of ID (PFOID) for controlling a quadcopter in the presence of uncertain parameters and external disturbances. Using the proposed controller the system's capacity to achieve fast-tracking performance and accurate control over attitude and position is improved. To emphasize the effectiveness of the proposed controller, a comparison evaluation is performed with existing controllers SMCBS [Thanh and Hong, 2018]. The comparison demonstrates that the proposed strategy outperforms in trajectory tracking. Drawing motivation from the aforementioned works, the following is an overview of the key contributions of this article;

Proposes a novel sliding mode control (SMC) with backstepping (BS) based on a proportional fractional-order integral derivative (PFOID) sliding surface controller that successfully controls a quadcopter in the presence of uncertainties and disturbances. The primary goal of this controller is to effectively counteract and eliminate external disturbances (aerodynamic effect, sensor noise, external disturbance, wind effect, ground effect, and payload). By applying the proposed controller (PFOIDSMCBS), improved performance specifications are achieved, including faster settling time, low overshoot, reduced error, and minimized chattering effects compared to the SMCBS controller [Thanh and Hong, 2018]. Implementation of the proposed controller allows the quadcopter to achieve the desired trajectory with more accuracy, superior performance compared to the existing controllers, and the ability to effectively reduce tracking issues. The stability conditions of the system have been derived using Lyapunov stability criteria. Simulation scenarios were designed with high realism, aligning them closely with real-world applications such as transportation, agricultural spraying, etc.

The layout of the paper is as outlined: Section 1 starts with a brief overview, and Section 2 presents the quadcopter's dynamics, taking into account the wind and ground effects. Derivation of the controller and Lyapunov stability concept are given in Section 3, followed by implementation in Section 4, and Conclusion in Section 5.

2 Quadcopter Mathematical Modelling

2.1 Quadcopter Model

The section describes the quadcopter dynamics model [Kumar and Dewan, 2023]. The structure of the quadcopter is shown in Fig. 1, with their earth and body frames, as well as the rotational and translational motion directions.

This paper considers Φ, θ, and ψ (roll, pitch, and yaw) to be the angles of the quadcopter. The positions of the quadcopter are denoted by x, y, and z, and j_{xx}, j_{yy}, j_{zz} represent the relative inertial moments along the x, y, and z axes, respectively.

The linear and angular velocities of the body frame (B_f) are denoted as;

$$v_l = [u_l, v_l, w_l]^T \quad \text{(m/s)},$$

$$v_r = [u_r, v_r, w_r]^T \quad \text{(rad/s)}.$$

This section describes a transformation matrix $\mathbf{M}_{\text{tra}}$ and a rotational matrix $\mathbf{M}_{\text{rot}}$ from the body frame (B_f) to the earth frame (E_f) and vice versa using the Euler angles method. This method, introduced by Leonhard Euler, is well-understood and easy to implement.

The rotational matrices for the roll (Φ), pitch (θ), and yaw (ψ) angles are defined as follows:

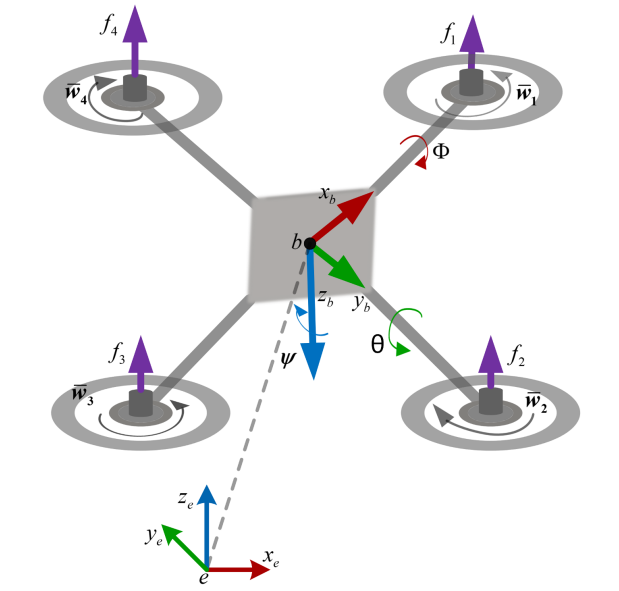

Figure 1. Quadcopter Model

$$\mathbf{M}_{\text{rotx}}(\Phi) = \begin{bmatrix} 1 & 0 & 0 \\ 0 & \cos(\Phi) & -\sin(\Phi) \\ 0 & \sin(\Phi) & \cos(\Phi) \end{bmatrix},$$

$$\mathbf{M}_{\text{roty}}(\theta) = \begin{bmatrix} \cos(\theta) & 0 & \sin(\theta) \\ 0 & 1 & 0 \\ -\sin(\theta) & 0 & \cos(\theta) \end{bmatrix},$$

$$\mathbf{M}_{\text{rotz}}(\psi) = \begin{bmatrix} \cos(\psi) & -\sin(\psi) & 0 \\ \sin(\psi) & \cos(\psi) & 0 \\ 0 & 0 & 1 \end{bmatrix}.$$

The rotation and transformation matrix from the body frame (B_f) to the earth frame (E_f) is defined as:

$$\begin{aligned} \mathbf{M}_{\text{rot}} &= \mathbf{M}_{\text{rot}}(\psi, \theta, \Phi) \\ &= \begin{bmatrix} c_\theta c_\psi & s_\Phi s_\theta c_\psi - c_\Phi s_\psi & c_\Phi s_\theta c_\psi + s_\Phi s_\psi \\ c_\theta s_\psi & s_\Phi s_\theta s_\psi + c_\Phi c_\psi & c_\Phi s_\theta s_\psi - s_\Phi c_\psi \\ -s_\theta & s_\Phi c_\theta & c_\Phi c_\theta \end{bmatrix} \end{aligned} \quad (1)$$

The transformation matrix is defined as:

$$\mathbf{M}_{\text{tra}} = \begin{bmatrix} 1 & s_\Phi t_\theta & c_\Phi t_\theta \\ 0 & c_\Phi & -s_\Phi \\ 0 & \frac{s_\Phi}{c_\theta} & \frac{c_\Phi}{c_\theta} \end{bmatrix}.$$

Here, $s = \sin$, $c = \cos$, and $t = \tan$. Therefore, the dynamics are described using the Newton-Euler equations as follows [Nekoo et al., 2021]:

$$m(\mathbf{v}_r \times \mathbf{v}_l + \dot{\mathbf{v}}_l) = F_B - mgM_{\text{tra}}c_3 \quad (2)$$

$$\begin{aligned} \dot{\mathbf{v}}_l = \begin{bmatrix} \dot{u}_l \\ \dot{v}_l \\ \dot{w}_l \end{bmatrix} &= \begin{bmatrix} 0 \\ 0 \\ \frac{\eta_B}{m} \end{bmatrix} \begin{bmatrix} 0 & -w_r & v_r \\ w_r & c_\Phi & -u_r \\ -v_r & u_r & 0 \end{bmatrix} \begin{bmatrix} u_l \\ v_l \\ w_l \end{bmatrix} \\ &\quad - g \begin{bmatrix} -s_\theta \\ c_\theta s_\Phi \\ c_\theta c_\Phi \end{bmatrix} \begin{bmatrix} 0 \\ 0 \\ 1 \end{bmatrix} \end{aligned}$$

Considered in the hover state, the rotation of the body coordinate relative to the inertial frame; therefore, it is approximated that

$$\dot{\mathbf{M}}_{\text{rot}}\mathbf{v}_l + \mathbf{M}_{\text{rot}}\dot{\mathbf{v}}_l \approx \dot{\mathbf{v}}_l.$$

Then, the gravity and $\mathbf{F}_B$ are transformed into the body frame B_f.

The equation for $\dot{\mathbf{v}}_l$ is given by:

$$\begin{aligned} \dot{\mathbf{v}}_l = \begin{bmatrix} \dot{u}_l \\ \dot{v}_l \\ \dot{w}_l \end{bmatrix} &= \begin{bmatrix} c_\Phi s_\theta c_\psi + s_\Phi s_\psi \\ c_\Phi s_\theta c_\psi - s_\Phi c_\psi \\ c_\Phi c_\theta \end{bmatrix} \frac{\tau_B}{m} \\ &\quad - \begin{bmatrix} 0 & -w_r & v_r \\ w_r & c_\Phi & -u_r \\ -v_r & u_r & 0 \end{bmatrix} \begin{bmatrix} u_l \\ v_l \\ w_l \end{bmatrix} - \begin{bmatrix} 0 \\ 0 \\ g \end{bmatrix} \\ &\quad - \frac{1}{m} \begin{bmatrix} j_{xx} & 0 & 0 \\ 0 & j_{yy} & 0 \\ 0 & 0 & j_{zz} \end{bmatrix} \begin{bmatrix} \dot{x}_B \\ \dot{y}_B \\ \dot{z}_B \end{bmatrix} \end{aligned} \quad (3)$$

$$\hat{\mathbf{v}}_{\text{rot}} = \begin{bmatrix} 0 & -w_r & v_r \\ w_r & 0 & -u_r \\ -v_r & u_r & 0 \end{bmatrix}$$

$$\mathbf{j} = \text{diag}(j_{xx}, j_{yy}, j_{zz})$$

τ_B: Thrust of the propeller in ground effect, $\mathbf{F}_B$: Input force vector.

In the body frame, the rotational dynamic is:

$$\mathbf{j}\dot{\mathbf{v}}_{\text{rot}} + \mathbf{v}_{\text{rot}} \times \mathbf{j}\mathbf{v}_{\text{rot}} = \mathbf{u}_B$$

where $\mathbf{j}$ is the identity matrix.

$$\begin{aligned} \dot{\mathbf{v}}_r = \begin{bmatrix} \dot{u}_r \\ \dot{v}_r \\ \dot{w}_r \end{bmatrix} &= \begin{bmatrix} \frac{I_\Phi}{j_{xx}} \\ \frac{I_\theta}{j_{yy}} \\ \frac{I_\psi}{j_{zz}} \end{bmatrix} \\ &\quad - \mathbf{j}^{-1} \begin{bmatrix} 0 & -w_r & v_r \\ w_r & c_\Phi & -u_r \\ -v_r & u_r & 0 \end{bmatrix} \begin{bmatrix} j_{xx} & 0 & 0 \\ 0 & j_{yy} & 0 \\ 0 & 0 & j_{zz} \end{bmatrix} \begin{bmatrix} u_r \\ v_r \\ w_r \end{bmatrix} \end{aligned} \quad (4)$$

Using the 4 rotors, thrust and moment are produced in the quadcopter's with rotating at an angular speed $\bar{\omega}(t)$ (rad/s). So, the angular velocity of the rotors is:

$$\bar{\omega}(t) = \sqrt{\left(\begin{bmatrix} k & k & k & k \\ 0 & -lk & 0 & k \\ -lk & 0 & lk & 0 \\ -K_c & K_c & -K_c & K_c \end{bmatrix}^{-1} \begin{bmatrix} I_z \\ I_\Phi \\ I_\theta \\ I_\psi \end{bmatrix} \right)} \quad (5)$$

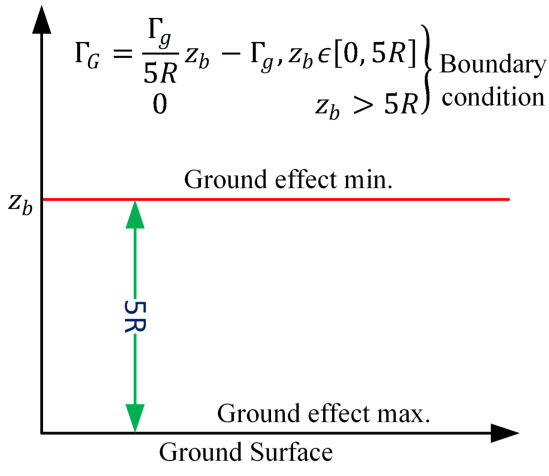

Figure 2. Ground effect region

2.2 Ground modelling

In the flight stage, the quadcopter approaches the surface (near the landing), and the thrust is turned off. Then, the quadcopter loses its controllability and drops to the surface. Therefore, quadcopter landing time is not guaranteed. For a quadcopter to land on a fixed point, the accuracy of the landing time is crucial.
The ground effect equation derived in [Sanchez-Cuevas et al., 2017] with a relation for calculating thrust close to the ground;

$$\frac{\tau_g}{\tau_B} = \frac{1}{1 - \left(\frac{R}{4z_b}\right)^2 - \frac{R^2 z_b}{\sqrt{(d+4z_b^2)^3}} - \frac{R^2 z_b}{\sqrt{2\left(2d+4z_b^2\right)^3}}} \quad (6)$$

$$\tau_g = 2\rho A_o \Gamma_g^2, \quad \tau_B = 2\rho A_o \Gamma_o^2$$

Eq. (6) represents the ground reflection of wind with direction towards the ground $-z$, thus the negative sign for Γ_g:

$$\frac{\tau_g}{\tau_B} = \frac{1}{1 - \left(\frac{R}{4z_b}\right)^2 - \frac{R^2 z_b}{\sqrt{(d+4z_b^2)^3}} - \frac{R^2 z_b}{\sqrt{2\left(2d+4z_b^2\right)^3}}} \quad (7)$$

There will be some wind loss due to turbulence and interference of the airflows by rotors, though the maximum reflection $\Gamma_G \leq \Gamma_g$ is always less than Γ_g. Therefore, the controller design based on Eq. (7) is safe and covers the ground wind reaction since Γ_g, in reality, is less than the theoretical design.
τ_g: Thrust of propeller outside ground effect, Γ_o: Air velocity far from the ground, Γ_g: Air velocity near to the ground, Γ_G: Air velocity reflected to the ground.

Figure 2 represents the maximum and minimum region of ground effect with boundary conditions. To achieve a smooth and soft landing without relying on specialized landing gear, it's essential to account for the wind reflection generated by the ground in the controller design and system modeling.

2.3 Wind Modelling

Wind velocity coordinates of the quadcopter are defined as $\bar{\mathbf{w}} = \begin{bmatrix} w_x & w_y & w_z \end{bmatrix}^T$ (m/s) [Nekoo et al., 2021]. Transforming the wind coordinate to the body frame of the quadcopter, the translation matrix is:

$$\bar{\mathbf{w}}(t) = d_i^w = \begin{bmatrix} w_x & w_y & w_z \end{bmatrix}^T = R_{zxy}^T(r_2)\mathbf{w} \quad (8)$$

$$\bar{\mathbf{w}}(t) = \begin{bmatrix} 0 & 0 & \Gamma_G(t) \end{bmatrix} \text{ [Lungu, 2020]}, \quad (9)$$

for a soft landing of the quadcopter on the ground.

2.4 Disturbances

The robustness of the controller was verified by adding various disturbances to the quadcopter's dynamic: aerodynamic effect d_i^a (i.e., $\sin(2t)$); random noise d_i^s is added as random noise (lie 0 to 1); external disturbance d_i^e [Kumar and Dewan, 2023] are defined as:

$$\begin{bmatrix} d_\phi^{en}(t) = d_\theta^{en}(t) = 7 + 2\cos\left(\frac{2\pi}{3}t\right), \\ d_\psi^{en}(t) = 5 + 2\cos\left(\frac{\pi}{2}t\right), \\ d_x^{en}(t) = d_y^{en}(t) = d_z^{en}(t) = 18 + 4\cos\left(\frac{\pi}{6}t\right) \end{bmatrix}$$

Total external disturbances written as:

Translation motion;

$$d_{\text{tri}} = d_i^a + d_i^s + d_i^e + d_i^{pu} + d_i^w$$

where $i = x, y, z$. Rotational motion:

$$d_{\text{roi}} = d_i^a + d_i^s + d_i^e + d_i^{pu} + d_i^w \quad (10)$$

where $i = \Phi, \theta, \psi$. Furthermore, parametric uncertainties were added to the system. This represents a 20% mass variation that can be included in the landing load drop and hovering dynamics.

3 Controller design

This section introduces a controller design that addresses the control of the quadcopter rotation and translation motion in the presence of model uncertainties and disturbances. The quadcopter dynamics are nonlinear and underactuated because it has 4

Table 1. Physical Parameters

Parameters	Name	Value/Unit
m	Mass	0.23 kg
$j_{xx} = j_{yy}$	Moment of inertia in the x and y-axis	7.5×10^(-3) kgm^2
j_{zz}	Moment of inertia in the z-axis	1.3×10^(-2) kgm^2
Ω_r	Rotor inertia	6×10^(-2) kgm^2
k	Thrust coefficient	3.13×10^(-5) Nms^2
k_c	Drag Coefficient	7.5×10^(-7) Nms^2
l	Length	0.23 m
R	Radius of the propellers	0.075 m
A_o	Air density	1.225km/m^3

control inputs (I_z, I_Φ, I_θ, I_ψ) and 6 outputs (x, y, z, Φ, θ, ψ).

The state-space form representation of the dynamic model of the quadcopter is [Kumar and Dewan, 2023]:

$$\dot{X} = f(X,u) + d(X,u)$$

where X, d, and u are the state, disturbances, and input vectors, respectively.

$$X = \begin{bmatrix} x_1 & x_2 & x_3 & x_4 & x_5 & x_6 & x_7 & x_8 & x_9 & x_{10} \\ x_{11} & x_{12} \end{bmatrix}^T$$

$$= \begin{bmatrix} \Phi & \dot{\Phi} & \theta & \dot{\theta} & \psi & \dot{\psi} & z & \dot{z} & x & \dot{x} \\ y & \dot{y} \end{bmatrix}^T \in \mathbb{R}^{12}$$

$$\dot{X} = \begin{bmatrix} \dot{x}_1 = \dot{\Phi} = x_2 \\ \dot{x}_2 = \ddot{\Phi} = a_1\dot{\theta}\dot{\psi} + a_2\ddot{\theta}\Omega_r + b_\Phi I_\Phi + d_{ro\Phi} \\ \dot{x}_3 = \dot{\theta} = x_4 \\ \dot{x}_4 = \ddot{\theta} = a_3\dot{\psi}\dot{\Phi} + a_4\ddot{\Phi}\Omega_r + b_\theta I_\theta + d_{ro\theta} \\ \dot{x}_5 = \dot{\psi} = x_6 \\ \dot{x}_6 = \ddot{\psi} = a_5\dot{\Phi}\dot{\theta} + b_\psi I_\psi + d_{ro\psi} \\ \dot{x}_7 = \dot{z} = x_8 \\ \dot{x}_8 = \ddot{z} = -g + (\delta_z)\frac{I_z}{m} + d_{roz} \\ \dot{x}_9 = \dot{x} = x_{10} \\ \dot{x}_{10} = \ddot{x} = (\delta_x)\frac{I_x}{m} + d_{rox} \\ \dot{x}_{11} = \dot{y} = x_{12} \\ \dot{x}_{12} = \ddot{y} = (\delta_y)\frac{I_y}{m} + d_{roy} \end{bmatrix} \quad (11)$$

The parameters are defined as:

$$a_1 = \frac{(j_{yy} - j_{zz})}{j_{xx}}, \quad a_2 = \frac{j_r}{j_{xx}}, \quad a_3 = \frac{(j_{zz} - j_{xx})}{j_{yy}},$$

$$a_4 = \frac{j_r}{j_{yy}}, \quad a_5 = \frac{(j_{xx} - j_{yy})}{j_{zz}}$$

$$b_\Phi = \frac{l}{j_{xx}}, \quad b_\theta = \frac{l}{j_{yy}}, \quad b_\psi = \frac{1}{j_{zz}}$$

$$\delta_x = \sin(\theta)\cos(\Phi)\cos(\psi) + \sin(\Phi)\sin(\psi),$$

$$\delta_y = \sin(\theta)\cos(\Phi)\cos(\psi) - \sin(\Phi)\sin(\psi),$$

$$\delta_z = \cos(\theta)\cos(\Phi)$$

The block diagram scheme of the controller is shown in Figure. 3.

Factors considered for designing a controller are

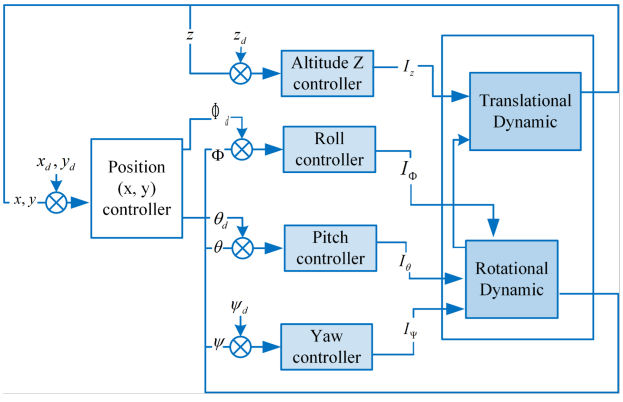

Figure 3. Controller Scheme diagram of the quadcopter

simple, robust, and provide good tracking performance without requiring information on the top range of the disturbances. The general sliding mode control law is:

$$I_i^+ = I_{eqvi} + I_{si} \quad (12)$$

I_{eqvi} is the input/output linearization and I_{si} is the switching control law, which provides additional control effort to minimize tracking errors and the effect of disturbances.

3.1 Design a proportional–fractional order–integral–derivative sliding surface sliding mode control with backstepping

For choice of sliding surface procedure; tracking error (e_i) for SMC with BS [Bouabdallah and Siegwart, 2005] is;

$$e_i = x_{id} - x_i, \quad i \in \{1,3,5,7,9,11\}$$

$$\dot{e}_i = \dot{x}_i - \dot{x}_{(i-1d)} - \gamma_{(i-1)} e_{(i-1)}, \quad i \in \{2,4,6,8,10,12\}$$

$$\ddot{e}_i = \dot{x}_2 - \ddot{x}_{1d} - \gamma_1 \dot{e}_1 \quad \text{with } 0 < \gamma_i < \infty \quad (13)$$

Considering the Lyapunov function is:

$$V_i = \frac{1}{2} e_i^2, \quad i \in \{1,3,5,7,9,11\}$$

$$V_i = \frac{1}{2}(s_{(i-1)} + e_i^2), \quad i \in \{2,4,6,8,10,12\} \quad (14)$$

These satisfy the necessary sliding condition $\dot{S} < 0$. Let's take the PFOID as a sliding surface, and its equation is based on the literature [Mian and Daobo, 2008],[Saini and Ohri, 2023]. The first-order equation of the PID sliding surface is:

$$\ddot{s}_i + \eta_i \dot{s}_i = k_{p_i} \dot{e}_i + k_{i_i} e_i + k_{d_i} \ddot{e}_i, \quad \eta_i \in \mathbb{R}^+$$

Convert into the form of PFOID (with the second derivate);

$$\ddot{s}_i + \eta_i \dot{s}_i = k_{p_i} \dot{e}_i + k_{i_i}^{\mu} e_i + k_{d_i}^{\sigma} \ddot{e}_i \quad (15)$$

Here, $I_i = \{i = (2 = \Phi, 4 = \theta, 6 = \psi)\}$ is the control input for the rotational subsystem, and $I_i = \{i = (8 = z, 10 = x, 12 = y)\}$ is the control input for the translational subsystem of the quadcopter.

Calculation for roll:

Let i=1,2 Surface are;

$$e_1 = x_{1d} - x_1$$

$$S_2 = e_2 = x_2 - \dot{x}_{1d} - \gamma_1 e_1 \quad (16)$$

and Lyapunov function is;

$$V(e_1, S_2) = \frac{1}{2}\left(e_1^2 + S_2^2\right)$$

Applying the condition $S\dot{S}<0$ for the surface, makes the following:

$$\begin{aligned} \dot{s}_2 &= -\beta_1 \,\text{sign}(s_2) - \alpha_2 s_2 \\ &= \dot{x}_2 - \ddot{x}_{1d} - \gamma_1 \dot{e}_1 \\ &= a_1 \dot{\theta}\dot{\psi} + a_2 \ddot{\theta}\Omega_r + b_\Phi I_\Phi + d_{ro\Phi} - \ddot{x}_{1d} - \gamma_1(e_2 + \gamma_1 e_2) \end{aligned} \quad (17)$$

Converting eq. (14) in terms of roll ;

$$\ddot{s}_2 + \eta_\Phi \dot{s}_2 = k_{p\Phi} \dot{e}_2 + k_{i\Phi}^{\mu} e_2 + k_{d\Phi}^{\sigma} \ddot{e}_2 \quad (18)$$

Using the eq. (17) and put the value of $\ddot{e}_2$ from (10) and (16);

$$\begin{aligned} &\ddot{s}_2 + \eta_\Phi \dot{s}_2 = \\ &\quad k_{p\Phi} \dot{e}_2 + k_{i\Phi}^{\mu} e_2 + k_{d\Phi}^{\sigma} \Big(a_1 \dot{\theta}\dot{\psi} + a_2 \ddot{\theta}\Omega_r \\ &\quad + b_\Phi I_\Phi + d_{ro\Phi} - \ddot{x}_{1d} - \gamma_1(e_2 + \gamma_1 e_2)) \end{aligned} \quad (19)$$

For the essential condition $\ddot{s}_2 = 0$, for tracking error to remain on the sliding surface and external disturbance is zero $d_{ro\Phi} = 0$;

$$\begin{aligned} I_\Phi = \frac{1}{b_\Phi k_{d\Phi}^{\sigma}} &(-\eta_\Phi \dot{s}_2 + k_{p\Phi} \dot{e}_2 + k_{i\Phi}^{\mu} e_2 \\ &+ k_{d\Phi}^{\sigma} \Big(a_1 \dot{\theta}\dot{\psi} + a_2 \ddot{\theta}\Omega_r - \ddot{x}_{1d} - \gamma_1(e_2 + \gamma_1 e_2) \Big) \end{aligned} \quad (20)$$

Now added the disturbance and the switching function [Fang et al., 2010] in eq. (19);

$$\begin{aligned} I_\Phi = \frac{1}{b_\Phi k_{d\Phi}^{\sigma}} &(-\eta_\Phi \dot{s}_2 + k_{p\Phi} \dot{e}_2 + k_{i\Phi}^{\mu} e_2 \\ &+ k_{d\Phi}^{\sigma} \Big(a_1 \dot{\theta}\dot{\psi} + a_2 \ddot{\theta}\Omega_r + d_{ro\Phi} \\ &- \ddot{x}_{1d} - \gamma_1(e_2 + \gamma_1 e_1) + (-\beta_1 \text{sign}(s_2) - \alpha_2 s_2) \end{aligned} \quad (21)$$

$\ddot{s}_2$ is calculated by substituting eq. (20) in (19)

$$\ddot{s}_2 = -k_{d\Phi}^{\sigma} d_{ro\Phi} - b_\Phi k_{d\Phi}^{\sigma} \alpha_2 s_2 - b_\Phi k_{d\Phi}^{\sigma} \beta_1 \,\text{sign}(s_2) \quad (22)$$

Converting, $\ddot{s}_2$ into the generalization from $\ddot{s}_i$, for i = 2, 4, 6, 8, 10, 12;

$$\ddot{s}_i = -k_{di}^{\sigma} d_{ro_i} - b_i k_{di}^{\sigma} \alpha_i s_i - b_i k_{di}^{\sigma} \beta_i \,\text{sign}(\dot{s}_i) \quad (23)$$

where

$$\text{sign}(\dot{s}(t)) = \begin{cases} +1, & \text{if } \dot{s}(t) > 0 \\ 0, & \text{if } \dot{s}(t) = 0 \\ -1, & \text{if } \dot{s}(t) < 0 \end{cases}$$

Then modified eq. (22) with the disturbance;

$$I_\Phi^+ = \frac{1}{b_\Phi k_{d\Phi}^{\sigma}} \begin{pmatrix} -\eta_\Phi \dot{s}_2 + k_{p\Phi} \dot{e}_2 + k_{i\Phi}^{\mu} e_2 \\ +k_{d\Phi}^{\sigma} \begin{pmatrix} a_1 \dot{\theta}\dot{\psi} + a_2 \ddot{\theta}\Omega_r - \ddot{x}_{1d} \\ +d_{ro\Phi} - \gamma_1 \\ (\dot{e}_2 + \gamma_1 e_1) \end{pmatrix} \\ -\beta_1 \,\text{sign}(s_2) - \alpha_2 s_2 \end{pmatrix} \quad (24)$$

Other control inputs for rotational and translational subsystems are calculated on the same lines and are defined as;

$$I_\theta^+ = \frac{1}{b_\theta k_{d\theta}^\sigma}\begin{pmatrix} -\eta_\theta \dot{s}_3 + k_{p\theta}\dot{e}_4 + k_{i\theta}^\mu e_4 \\ +k_{d\theta}^\sigma \begin{pmatrix} a_3\dot{\psi}\dot{\Phi} + a_4\ddot{\Phi}\Omega_r - \ddot{x}_{3d} \\ +d_{ro\theta} - \gamma_2 \\ (e_4 + \gamma_2 e_3) \end{pmatrix} \\ -\beta_3\,\text{sign}(s_3) - \alpha_4 s_3 \end{pmatrix} \tag{25}$$

$$I_\psi^+ = \frac{1}{b_\psi k_{d\psi}^\sigma}\begin{pmatrix} -\eta_\psi \dot{s}_4 + k_{p\psi}\dot{e}_6 + k_{i\psi}^\mu e_6 \\ +k_{d\psi}^\sigma \begin{pmatrix} a_5\dot{\Phi}(\dot{\theta}) - \ddot{x}_{5d} \\ +d_{ro\psi} - \gamma_3 \\ (e_6 + \gamma_3 e_5) \end{pmatrix} \\ -\beta_5\,\text{sign}(s_4) - \alpha_6 s_4 \end{pmatrix} \tag{26}$$

3.2 Stability Interpretation

Theorem 1: In the paper, the sliding surface is defined by equation (22) and the control law I_Φ, I_θ, I_ψ, I_z is defined by equations (23), (24), (25), and (26). The system is asymptotically stable if $\dot{V}_i < 0$ (i.e., it is negative definite). For a positive definite differential quadratic Lyapunov function [Kumar and Dewan, 2023] defined as:

$$V_i = \frac{1}{2}s_i^2 + \frac{1}{2}\dot{s}_i^2 \quad \text{with} \quad \begin{cases} V_i(0) = 0 \\ V(t) > 0 \quad \text{for} \quad s_i \to \text{(i = 2, 3, 4)} \end{cases} \tag{27}$$

Proof 1: For roll, pitch, and yaw
Differentiating eq. (29) w.r.t time and substituting (22)

$$\dot{V}_i = s_i\dot{s}_i + \dot{s}_i\ddot{s}_i \tag{28}$$

$$\dot{V}_i = s_i\dot{s}_i + \dot{s}_i\left(-k_i^\sigma d_{r_{oi}} - b_i k_i^\sigma \alpha_i s_i - b_i k_i^\sigma \beta_i\,\text{sign}(\dot{s}_i)\right)$$

$$\dot{V}_i = \dot{s}_i\left(s_i - k_i^\sigma d_{r_{oi}} - b_i k_i^\sigma \alpha_i s_i - b_i k_i^\sigma \beta_i\,\text{sign}|\dot{s}_i|\right)$$

$$\dot{V}_i \le |\dot{s}_i|\left(s_i - k_i^\sigma d_{r_{oi}} - b_i k_i^\sigma \alpha_i s_i - b_i k_i^\sigma \beta_i|\dot{s}_i|\right)$$

$$\dot{V}_i \le |\dot{s}_i|\left(s_i\left(1 - b_i k_i^\sigma \alpha_i\right) + k_i^\sigma\left(d_{r_{oi}}^+ - b_i\beta_i\right)|\dot{s}_i|\right)$$

Where $d_{r_{oi}}^+ \in \mathbb{R}^+$ is the upper bound on disturbance [Thanh and Hong, 2018]. For asymptotic stability, $\dot{V}_i < 0$;
$\dot{V}_i$ will always be negative if:

$$\begin{cases} \alpha_i > \frac{1}{b_i k_{di}^\sigma}, & \alpha_i \text{ for } i = 2, 4, 6 \\ \beta_i > \frac{d_{r_{oi}}^+}{b_i}, & \beta_i \text{ for } i = 1, 3, 5 \end{cases} \tag{29}$$

Proof 2: for z
Using the eq. (22) and put the value $\ddot{s}_5$ that is found out by taking the same approach as $\ddot{s}_2$, that is;

$$\ddot{s}_5 = -k_{dz}^\sigma d_{trz} - k_{dz}^\sigma \alpha_z s_5 - k_{dz}^\sigma \beta_7\,\text{sign}(\dot{s}_5)$$

Now,

$$\dot{V}_i = s_5\dot{s}_5 + \dot{s}_5\ddot{s}_5$$

$$\dot{V}_i = s_5\dot{s}_5 + \dot{s}_5\left(-k_{dz}^\sigma d_{trz} - k_{dz}^\sigma \alpha_8 s_5 - k_{dz}^\sigma \beta_7\,\text{sign}(\dot{s}_5)\right)$$

$$\dot{V}_i = \dot{s}_5\left(s_5 - k_{dz}^\sigma d_{trz} - k_{dz}^\sigma \alpha_8 s_5 - k_{dz}^\sigma \beta_7|\dot{s}_5|\right)$$

$$\dot{V}_i \le |\dot{s}_5|\left(s_5 - k_{dz}^\sigma \alpha_8 s_5 - k_{dz}^\sigma d_{trz} - k_{dz}^\sigma \beta_7|\dot{s}_5|\right)$$

$$\dot{V}_i \le |\dot{s}_5|\left(s_5\left(1 - k_{dz}^\sigma \alpha_8\right) + k_{dz}^\sigma\left(d_{trz}^+ - \beta_7\right)|\dot{s}_5|\right)$$

Where $d_{trz}^+ \in \mathbb{R}^+$ is the upper bound of disturbance. For asymptotic stability, $\dot{V}_i < 0$, and $\dot{V}_i$ will always be negative if:

$$\begin{cases} \alpha_8 > \frac{1}{k}{}^\sigma_{dz} \\ \beta_7 > d_{trz}^+ \end{cases} \tag{30}$$

Given that V_i is negative definite, all system state trajectories will converge to and remain on the corresponding sliding surfaces under the specified control laws.

4 Simulation results and discussion

The effectiveness and strength of the proposed controller (PFOID surface-based SMCBS) for attitude, altitude, and position control under external disturbances, ground effects, and payload are discussed in this section. Physical parameter values of the quadcopter are given in Table 1. The sliding gains were determined by the hit-and-trail method and the gain of the PID controller by the ultimate gain method (Table 2).
The total time interval (T) of the tracking trajectory of the quadcopter is from 0 to 35 seconds. The quadcopter traveling time has been divided into three intervals, as shown in Figure 3.

1. T_1 (0-15 seconds), a fixed point at 1.0 m height for hover state.
2. T_2 (15-25 seconds), the quadcopter lands from 1.0 m to 0.2 m.
3. T_3 (25-35 seconds), the quadcopter returns to a hover state at 1.2 m.

Aerodynamic drag, random noise, external disturbances, wind effects, ground effects, and mass variation due to payload discussed in Section 2 have been taken into account dynamically. The ground effect is significant only during the low-altitude flight of the vehicle ($< 5R = 0.375$, Figure 2). The landing set point is chosen < 0.2 m

Table 2. Controller Parameters

Variable	Definition	x	y	z	ϕ	θ	ψ
k_p	Proportional	4.9	4.9	11.0	8.0	8.0	8.0
k_i	Integral	0.68	0.68	1.01	1.33	1.44	0.89
k_d	Derivative	0.66	0.66	0.14	0.33	0.33	0.11
η	Constant Surface	2.0	2.0	2.0	1.0	1.0	3.0
α	Sliding Function	20.0	20.0	20.0	17.0	17.0	20.0
β		3.69	3.69	3.69	2.56	2.56	3.20
μ	Fractional order	0.8	0.8	0.8	0.8	0.8	0.8
σ		0.64	0.64	0.64	0.64	0.64	0.64

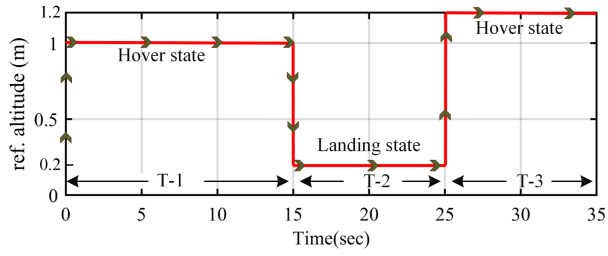

Figure 4. Reference Trajectory

4.1 SIMULATION RESULTS

Simulation has been done for two scenarios.

Scenario 1: Flight tracking under disturbances, wind, and ground effect.
Scenario 2: Flight tracking under disturbances, wind and ground effect, and payload.

Scenario 1: During the first time interval, T-1; Quadcopter takes off from 0.0 m to achieve the height of 1.0 m after receiving the command. Ground effect is effective up to 5R=0.375. It tends to increase the rise time. The quadcopter reaches the desired altitude after 5.11 seconds in the case of the proposed controller and SMCBS controllers reach at 6.98 seconds. In T-2, the quadcopter lands at 0.2 m above the ground surface with the impact of the ground effect. The time taken by the proposed controller is 6.31 seconds, and SMCBS controllers are 8.14 seconds.

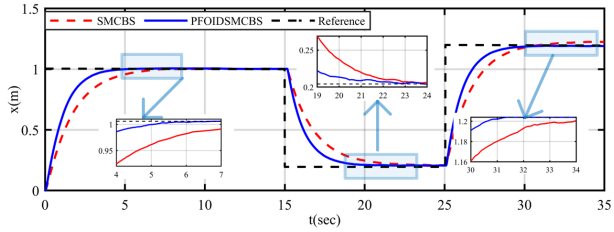

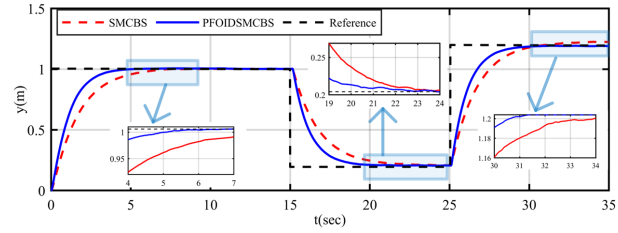

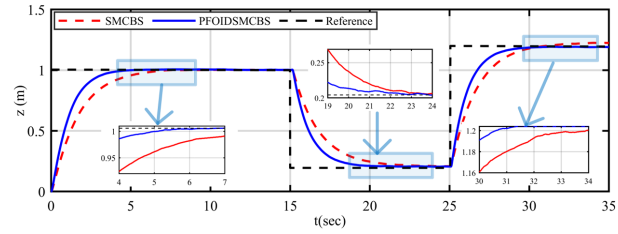

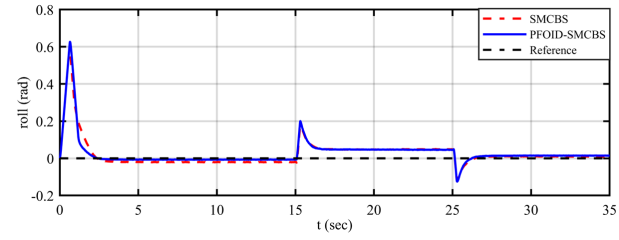

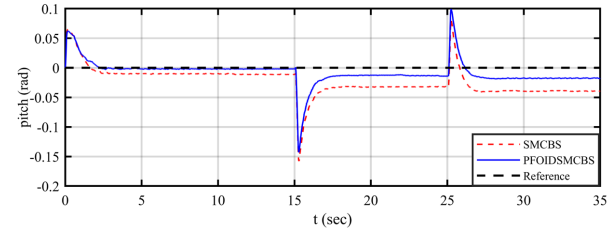

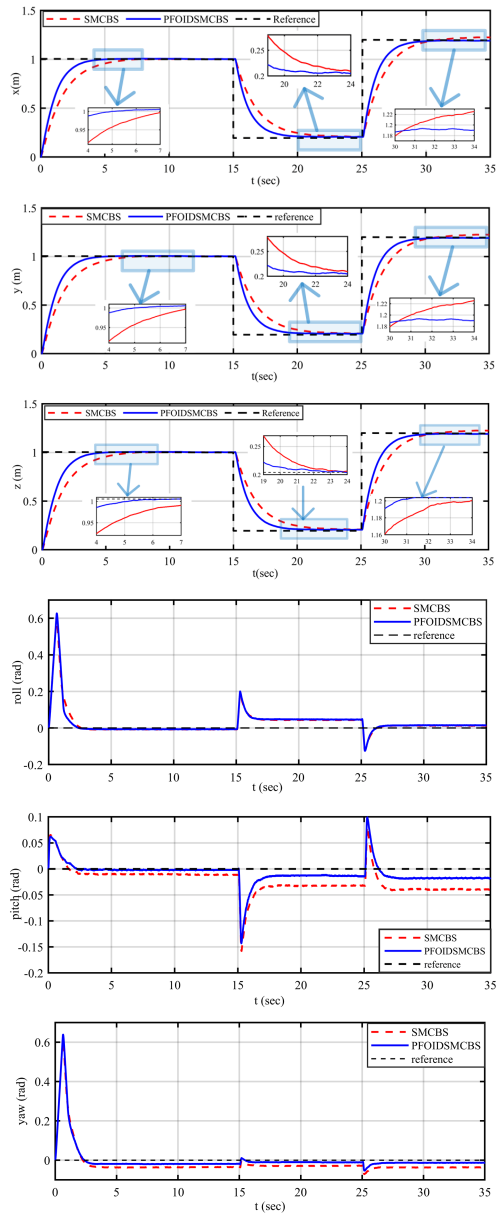

Figure 6. Performance comparison of the PFOIDSMCBS controller to SMCBS with various disturbances, wind effect, ground effect, and payload

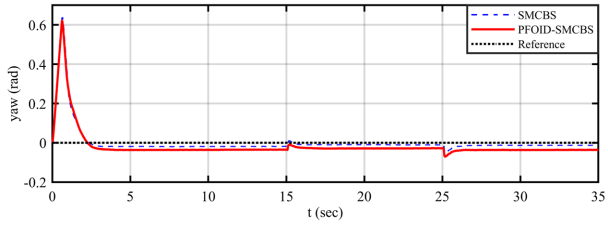

Figure 5. Performance comparison of the PFOIDSMCBS controller to SMCBS with various disturbances, wind effect, and ground effect

The quadcopter goes to a hover state from 0.2 m to 1.2 m in T-3 (t=25 to 35 seconds). SMCBS controllers take 8.44 seconds and proposed PFOIDSMCBS controllers take 5.32 seconds to complete the task. Performances specification for Figure 5 are quantified in Table 3. Performance has certainly improved by PFOIDSMCBS and the system is stable also as it satisfies stability criteria Table 6.

Scenario 2: This scenario is created based on the quadcopter's real-time applications. Considering, the quadcopter takes off with the payload (e.g. pesticide spray for agriculture) and sprays on the farm. After spraying, the quadcopter again goes to its original position. The other way around, the quadcopter lands on the ground picks up the payload, and returns to its position.

In case, (i) the quadcopter takes off with the payload (considering a +20% mass variation of the quadcopter), (ii) lands at 0.2 m near the field to spray, between 20 to 25 seconds, and then takes off without payload. From Figure. 6, in T-1, the quadcopter takes off from 0.0 m to achieve the height of 1.0 m with a +20% payload. The quadcopter reaches the desired altitude after 5.66 seconds in the case of the proposed controller and in the SMCBS controllers reaches 7.66 seconds. In T-2, the quadcopter lands at 0.2 m above the ground surface. Between 15 to 25 seconds, the quadcopter releases the payload slightly (in the agriculture spray process or parcel release process, etc.). The time taken by the proposed controller is 6.82 seconds, and the SMCBS controllers take 8.70 seconds.

The quadcopter goes to a hover state from 0.2 m to 1.2 m in T-3 (t = 25 to 35 seconds) with actual mass. SMCBS controllers take 8.24 seconds and proposed PFOIDSMCBS controllers take 5.22 seconds to complete the task. Performance specifications are quantified for Figure 6 in Table 4. Performance has certainly been improved by PFOIDSMCBS, and the system is stable also as it satisfies the stability criteria in Table 6.

From Table 3, it can be observed that the proposed controller during the landing state (time interval T-2) reduces the settling time by 6.12% as compared to the SMCBS of the system under no load. Additionally, the load is reduced by 5.17% from Table 4, in the z-direction.

From Figure 7, it is indicated that the proposed controller reduces chattering compared to the SMCBS controller. The proposed controller also requires less thrust during the quadcopter's hovering phase, indicating that it requires less control effort than the existing controller.

The proposed controller demonstrates performance in path tracking when compared to the existing SMCBS controller, even with a disturbed environment. Stability criteria are fulfilled according the eq. 31 and 32 from

Table 3. Performance specifications of the controller with various disturbances, wind effect, ground effect and no payload

Parameters	**Controllers**	**Time Interval (sec)**	**Variables**					
			x	y	z	ϕ	θ	ψ
Rise time	SMCBS	T-1 (0-15)	3.78	3.78	4.10	2.65	1.67	2.28
	PFOIDSMCBS	T-1 (0-15)	2.60	2.60	3.38	2.58	2.25	2.38
Overshoot Time	SMCBS	T-1 (0-15)	0	0	0	0.61	0.06	0.610
		T-2 (15-25)	0	0	0	0.199	-0.155	-0.011
		T-3 (25-35)	0	0	0	-0.120	0.08	-0.066
	PFOIDSMCBS	T-1 (0-15)	0	0	0	0.68	0.06	0.63
		T-2 (15-25)	0	0	0	0.199	-0.141	0.009
		T-3 (25-35)	0	0	0	-0.120	0.11	-0.046
Settling Time	SMCBS	T-1 (0-15)	7.42	7.92	7.98	2.65	1.67	2.18
		T-2 (15-25)	22.66	22.66	22.7	16.94	17.92	16.13
		T-3 (25-35)	32.94	32.94	33.24	26.23	25.83	26.82
	PFOIDSMCBS	T-1 (0-15)	5.01	5.01	5.11	2.65	2.15	2.18
		T-2 (15-25)	21.20	21.20	21.31	16.94	17.64	16.13
		T-3 (25-35)	29.82	29.82	30.32	26.23	25.83	26.12
Steady State Error	SMCBS	T-1 (0-15)	0.001	0.001	0.001	-0.007	-0.009	-0.035
		T-2 (15-25)	0.002	0.002	0.003	0.04	-0.032	-0.020
		T-3 (25-35)	0.002	0.002	0.004	0.0143	-0.038	-0.036
	PFOID SMCBS	T-1 (0-15)	0.004	0.004	0.004	-0.007	-0.002	-0.033
		T-2 (15-25)	0.002	0.002	0.002	0.044	-0.011	-0.009
		T-3 (25-35)	0.006	0.006	0.006	0.0143	-0.018	-0.066

Table 6; hence the system is asymptotically stable. According to the control law, every trajectory of the system's state will reach and stay on its designated sliding surface.

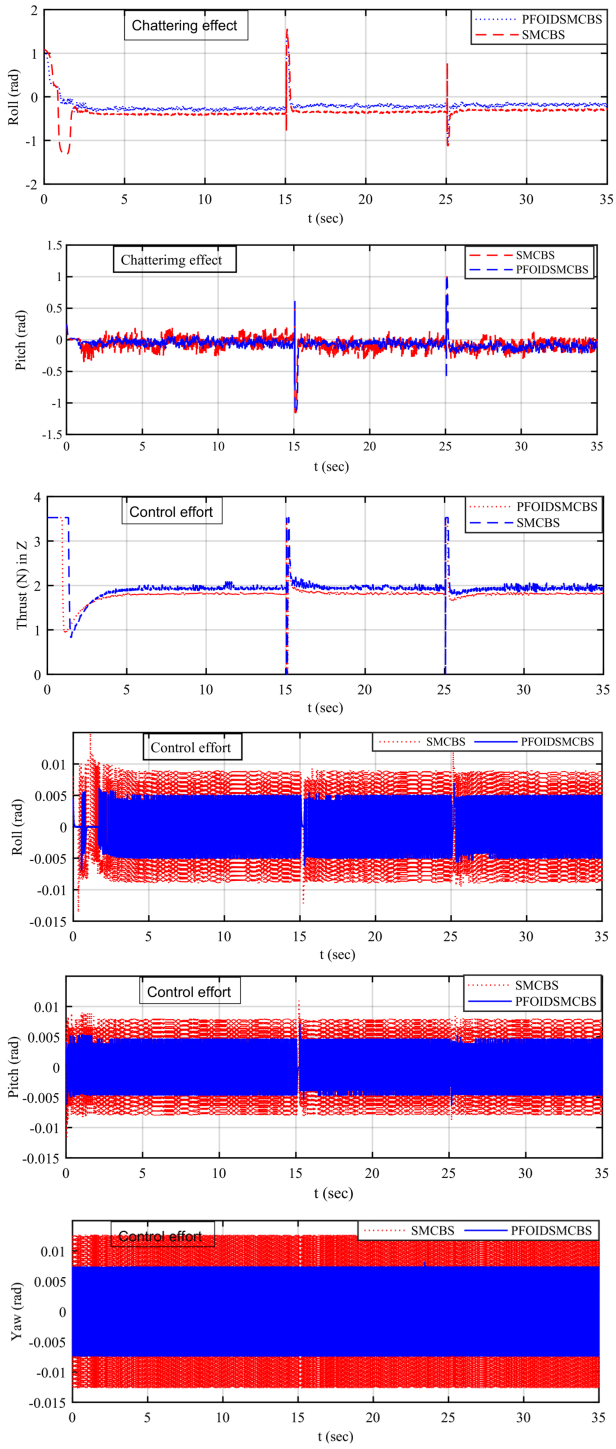

Figure 7. Chattering effect and control efforts

5 Conclusions

The paper proposed a hybrid controller (PFOIDSMCBS) for stabilizing the quadcopter to follow the predefined trajectory. To attain the robustness of the proposed controller; deployed in various disturbances (external disturbances, ground effect, wind effect, and mass variation) during takeoff, inflight, and landing and also compared with the existing controllers SMCBS and meets the stability requirements. Furthermore, in this study trajectory has been planned based on the quadcopters used in real-time applications. The quadcopter takes off to carry the payload (e.g., parcel, water or pesticide spray for agriculture, etc.) and drops/releases the payload to the ground. After the released payload, the quadcopter again goes to its original position. Respectively, the quadcopter takes off without the payload and lands on the ground. During to land quadcopter carries the load and returns to its position. The modelling outcomes demonstrate the effectiveness of the proposed controller in ensuring a soft landing for the quadcopter by mitigating the impact of thrust due to the ground effect. The wind deflected by the rotors near the ground generates extra thrust for the system, amending its planned trajectory to ensure a smooth landing. The controller successfully tracks the trajectory and achieves landing within a specified time frame, with no overshoot or undershoot. In the future, the proposed work could prove valuable for real-time drone missions.

References

Alexis, K., Nikolakopoulos, G., and Tzes, A. (2011). Switching model predictive attitude control for a quadrotor helicopter subject to atmospheric disturbances. *Control Engineering Practice*, **19** (10), pp. 1195–1207.

Ambati, P. R. and Padhi, R. (2014). A neuro-adaptive augmented dynamic inversion design for robust auto-landing. *IFAC Proceedings Volumes*, **47** (3), pp. 12202–12207.

Araar, O. and Aouf, N. (2014). Quadrotor control for trajectory tracking in presence of wind disturbances. In *2014 UKACC International Conference on Control (CONTROL)*, IEEE, pp. 25–30.

Ayad, R., Nouibat, W., Zareb, M., and Bestaoui Sebanne, Y. (2019). Full control of quadrotor aerial robot using fractional-order fopid. *Iranian Journal of Science and Technology, Transactions of Electrical Engineering*, **43**, pp. 349–360.

Bouabdallah, S. and Siegwart, R. (2005). Backstepping and sliding-mode techniques applied to an indoor micro quadrotor. In *Proceedings of the 2005 IEEE international conference on robotics and automation*, IEEE, pp. 2247–2252.

Chen, Y., He, Y., and Zhou, M. (2013). Modeling and control of a quadrotor helicopter system under impact of wind field. *Research Journal of Applied Sciences, Engineering and Technology*, **6** (17), pp. 3214–3221.

Cho, H., Udwadia, F. E., and Wanichanon, T. (2020). Autonomous precision control of satellite formation flight under unknown time-varying

Table 4. Performance specifications of the controller under various disturbances, mass variation, ground control, and payload

Parameters	Controllers	Time Interval (sec)	Variables					
			x	y	z	ϕ	θ	ψ
Rise time	SMCBS	T-1 (0-15)	3.67	3.67	3.96	2.65	1.67	2.28
	PFOID SMCBS	T-1 (0-15)	2.40	2.40	2.53	2.58	2.25	2.38
Overshoot Time	SMCBS	T-1 (0-15)	0	0	0	0.61	0.06	0.610
		T-2 (15-25)	0	0	0	0.199	-0.166	-0.011
		T-3 (25-35)	0	0	0	-0.120	0.08	-0.066
	PFOID SMCBS	T-1 (0-15)	0	0	0	0.68	0.06	0.63
		T-2 (15-25)	0	0	0	0.199	-0.122	0.011
		T-3 (25-35)	0	0	0	-0.120	0.11	-0.046
Settling Time	SMCBS	T-1 (0-15)	7.36	7.36	7.66	2.65	1.67	2.18
		T-2 (15-25)	22.89	22.89	23.01	17.91	18.39	16.99
		T-3 (25-35)	32.94	32.94	33.24	26.23	25.83	26.82
	PFOID SMCBS	T-1 (0-15)	4.95	4.95	5.22	2.65	2.15	2.18
		T-2 (15-25)	21.71	21.71	21.82	17.91	18.23	17.49
		T-3 (25-35)	29.82	29.82	30.32	26.23	25.83	26.12
Steady State Error	SMCBS	T-1 (0-15)	0.001	0.001	0.001	-0.007	-0.009	-0.035
		T-2 (15-25)	0.002	0.002	0.002	0.047	-0.036	-0.029
		T-3 (25-35)	0.002	0.002	0.002	0.0143	-0.038	-0.036
	PFOID SMCBS	T-1 (0-15)	0.004	0.004	0.004	-0.007	-0.002	-0.033
		T-2 (15-25)	0.002	0.002	0.002	0.047	-0.022	-0.099
		T-3 (25-35)	0.006	0.006	0.006	0.0143	-0.018	-0.066

Table 5. Stability Analysis

Parameter values	$\alpha_2 = 20$	$\alpha_4 = 20$	$\alpha_6 = 20$	$\alpha_8 = 20$	$\beta_1 = 2.56$	$\beta_3 = 3.20$	$\beta_5 = 3.20$	$\beta_7 = 3.69$
Parameter values	$\frac{1}{b_\phi k\sigma d_\phi} = 3.78$	$\frac{1}{b_\theta k\sigma} = 3.78$	$\frac{1}{b_\psi k\sigma d_\psi} = 5.56$	$\frac{1}{k\sigma d_z} = 1.25$	$\frac{d^+_{r\phi}}{b_\phi} = 0.71$	$\frac{d^+_{r\theta}}{b_\theta} = 0.57$	$\frac{d^+_{r\psi}}{b_\psi} = 2.35$	$d^+_{trz} = 1.67$

model and environmental uncertainties. *The Journal of the Astronautical Sciences*, **67** (4), pp. 1470–1499.

Danjun, L., Yan, Z., Zongying, S., and Geng, L. (2015). Autonomous landing of quadrotor based on ground effect modelling. In *2015 34th Chinese control conference (CCC)*, IEEE, pp. 5647–5652.

Davis, E., Spollard, J., and Pounds, P. (2015). Passive height stability and trajectory repeatability of a quadrotor maneuvering in ground effect with regulated voltage bus. In *Australasian Conference on Robotics and Automation, ACRA*, ARAA.

Dikmen, İ. C., Arisoy, A., and Temeltas, H. (2009). Attitude control of a quadrotor. In *2009 4th International Conference on Recent Advances in Space Technologies*, Ieee, pp. 722–727.

Fang, Z., Wang, X.-y., and Sun, J. (2010). Design and nonlinear control of an indoor quadrotor flying robot. In *2010 8th World Congress on Intelligent Control and Automation*, IEEE, pp. 429–434.

Fujita, M. and Shimada, A. (2007). Takeoff and landing control using force sensor by electrically-powered helicopters. *IEEJ Transactions on Industry Applications*, **127** (2), pp. 112–117.

Gao, G. and Wang, J. (2013). Reference command tracking control for an air-breathing hypersonic vehicle with parametric uncertainties. *Journal of the Franklin Institute*, **350** (5), pp. 1155–1188.

Hua, C., Chen, J., and Guan, X. (2019). Fractional-order sliding mode control of uncertain quavs with time-varying state constraints. *Nonlinear Dynam-*

ics, **95**, pp. 1347–1360.

Kumar, S. and Dewan, L. (2020). Different control scheme for the quadcopter: a brief tour. In *2020 First IEEE International Conference on Measurement, Instrumentation, Control and Automation (ICMICA)*, IEEE, pp. 1–6.

Kumar, S. and Dewan, L. (2022). Pfoid-smc approach to mitigate the effect of disturbance and parametric uncertainty on the quadcopter. *International Journal of Modelling, Identification and Control*, **40** (4), pp. 343–355.

Kumar, S. and Dewan, L. (2023). Quadcopter stabilization using hybrid controller under mass variation and disturbances. *Journal of Vibration and Control*, **29** (21-22), pp. 4857–4874.

Kumar, S. and Dewan, L. (2024). Hybrid controller for soft landing of a quadcopter. *IETE Journal of Research*, **70** (5), pp. 5100–5113.

Lungu, M. (2020). Backstepping and dynamic inversion combined controller for auto-landing of fixed wing uavs. *Aerospace Science and Technology*, **96**, pp. 105526.

Mian, A. A. and Daobo, W. (2008). Modeling and backstepping-based nonlinear control strategy for a 6 dof quadrotor helicopter. *Chinese Journal of Aeronautics*, **21** (3), pp. 261–268.

Mori, R., Hirata, K., Tamaki, T., and Yonezawa, N. (2008). Vision-based guidance control of a small-scale unmanned helicopter. *Journal of the Robotics Society of Japan*, **26** (8), pp. 905–912.

Nekoo, S. R., Acosta, J. Á., Heredia, G., and Ollero, A. (2021). Soft-landing of multi-rotor drones using a robust nonlinear control and wind modeling. In *2021 International Conference on Unmanned Aircraft Systems (ICUAS)*, IEEE, pp. 1070–1079.

Oliva-Palomo, F., Muñoz-Vázquez, A. J., Sánchez-Orta, A., Parra-Vega, V., Izaguirre-Espinosa, C., and Castillo, P. (2019). A fractional nonlinear pi-structure control for robust attitude tracking of quadrotors. *IEEE Transactions on Aerospace and Electronic Systems*, **55** (6), pp. 2911–2920.

Sadeghzadeh, I., Abdolhosseini, M., and Zhang, Y. (2014). Payload drop application using an unmanned quadrotor helicopter based on gain-scheduled pid and model predictive control. *Unmanned Systems*, **2** (01), pp. 39–52.

Sahrir, N. H. and Basri, M. A. M. (2023). Pso–pid controller for quadcopter uav: index performance comparison. *Arabian Journal for Science and Engineering*, **48** (11), pp. 15241–15255.

Saini, N. and Ohri, J. (2023). Load frequency control in three-area single unit power system considering non-linearities effect. *Cybern. Phys., no*, **12** (1), pp. 60–69.

Sanchez-Cuevas, P., Heredia, G., and Ollero, A. (2017). Characterization of the aerodynamic ground effect and its influence in multirotor control. *International Journal of Aerospace Engineering*, **2017** (1), pp. 1823056.

Sharf, I., Nahon, M., Harmat, A., Khan, W., Michini, M., Speal, N., Trentini, M., Tsadok, T., and Wang, T. (2014). Ground effect experiments and model validation with draganflyer x8 rotorcraft. In *2014 International Conference on Unmanned Aircraft Systems (ICUAS)*, IEEE, pp. 1158–1166.

Sharma, A. and Lather, J. S. (2020). Synchronization of coupled quadcopters using contraction theory. pp. 1–6.

Thanh, H. L. N. N. and Hong, S. K. (2018). Quadcopter robust adaptive second order sliding mode control based on pid sliding surface. *IEEE Access*, **6**, pp. 66850–66860.

Tran, N. K., Bulka, E., and Nahon, M. (2015). Quadrotor control in a wind field. In *2015 International Conference on Unmanned Aircraft Systems (ICUAS)*, IEEE, pp. 320–328.

Vahdanipour, M. and Khodabandeh, M. (2019). Adaptive fractional order sliding mode control for a quadrotor with a varying load. *Aerospace Science and Technology*, **86**, pp. 737–747.

Waslander, S. and Wang, C. (2009). Wind disturbance estimation and rejection for quadrotor position control. In *AIAA Infotech@ Aerospace conference and AIAA unmanned... Unlimited conference*, p. 1983.

Watanabe, K., Iwatani, Y., Nonaka, K., and Hashimoto, K. (2008). A visual-servo-based assistant system for unmanned helicopter control. In *2008 IEEE/RSJ International Conference on Intelligent Robots and Systems*, IEEE, pp. 822–827.

Xiong, J.-J. and Zheng, E.-H. (2014). Position and attitude tracking control for a quadrotor uav. *ISA transactions*, **53** (3), pp. 725–731.

Yacef, F., Bouhali, O., and Hamerlain, M. (2014). Adaptive fuzzy backstepping control for trajectory tracking of unmanned aerial quadrotor. In *2014 International Conference on Unmanned Aircraft Systems (ICUAS)*, IEEE, pp. 920–927.